# Reactive transport modeling of carbon capture in soil amended with fast weathering silicate minerals

**Reza Khalidy**
University of Guelph https://orcid.org/0000-0002-6769-9691
**Yi Wai Chiang**
University of Guelph https://orcid.org/0000-0002-7798-9166
**Rafael M. Santos** ( santosr@uoguelph.ca )
University of Guelph https://orcid.org/0000-0002-8368-8618

**Research Article**

**Keywords:** reactive transport modeling, enhanced rock weathering, soil inorganic carbon, pedogenic carbonate formation

**Posted Date:** January 12th, 2024

**DOI:** https://doi.org/10.21203/rs.3.rs-3851603/v1



**Additional Declarations:** The authors declare no competing interests.

## Abstract

Mineralization of powder form of fast-weathering silicate minerals (e.g., wollastonite and diopside) is reckoned as a stable and relatively low-cost method for sequestrating atmospheric $CO_2$ in agricultural and urban soils. While the process, called terrestrial enhanced weathering, has well shown the capacity of carbon drawdown in lab and field scale studies, the long-term evolution of formation/redissolution of weathering product is less discussed in the literature. This study assesses long-term carbonate formation and migration over the soil profile with a reactive transport model built within the Geochemist Workbench software package. The model is built on the basis of experimental design/ procedure conditions and accounts for intermittent irrigation regimes and kinetic dissolution/precipitation of minerals as well as calcite formation. Simulation results are indicative of the growth of sequestrated carbon beyond the short-term duration (up to 8.3 t $CO_2$/ha) with dissolved form (e.g., bicarbonates) growing over time. The model also predicts a slow migration of carbonates to deeper layers over five years. The modeling outputs are inconsistent with experimental observations, highlighting inflow rate as a driving factor in the formation of carbonates and mass of dissolved carbonate efflux from the system.

## 1. Introduction

To adhere to Paris agreement objective to limit global average temperature increase to 2°C compared to pre-industrial levels, there is an urgent need to develop large-scale carbon dioxide removal (CDR) technologies (Huang and Zhao, 2021; Campbell et al., 2022). As many conventional methods are costly, the focus should be on approaches that are executable on a large scale (La Plante et al., 2021; Wilson et al., 2014; Khalidy and Santos, 2021a). One of these methods, recently gaining the attention of researchers working in geochemistry and soil science, is Enhanced Rock Weathering (ERW), where the dissolution of fine silicate minerals enriched in divalent cations ($Ca^{2+}$ and $Mg^{2+}$) promotes the formation of stabilized carbonate over the long term (Rausis et al., 2022; Washbourne et al., 2015; Goll et al., 2021). It is estimated that large-scale practice of ERW can remove up to 2 to 10 Gt $CO_2$ annually (Beerling et al., 2020). Once in touch with agricultural lands, silicate minerals released during ERW profit plant-soil system and regulate the optimum pH range (Jariwala et al., 2022).

Accumulation of newly formed pedogenic carbonate due to ERW practice (e.g., the addition of wollastonite, olivine, and basalt) is well documented in the literature (Fatima et al., 2020; Kelland et al 2020, Khalidy et al., 2021; Jorat et al., 2022). The silicate mineral application rate is usually lower on the field scale (compared to laboratory experiments). However, previous studies reported that ERW can sequester up to 7 t $CO_2$/ha in field trials (Haque et al., 2020; Jorat et al., 2022). These findings call attention to executing large-scale ERW as a promising CDR method.

Nevertheless, it is only possible to investigate the fate of weathering products for a few months/years through field and laboratory experiments (Haque et al., 2020; Vienne et al., 2022). The timeline of lab/field experiments might not be long enough for whole silicate minerals to weather (Khalidy et al., 2023; Haque et al., 2023). Furthermore, the complexity of sampling in deep layers makes it burdensome to track the downward migration of newly formed carbonates in deeper horizons of soil. Hence, there is a need to track this process on a long-term scale to comprehend the mechanisms of migration of carbonates and quantifying the net capture of $CO_2$.

Reckoned as a practical technique, geochemical modeling has gained popularity as a predictive tool by scholars (Khalidy and Santos, 2021b). Several studies have employed geochemical modeling for simulating carbon capture through weathering in soils (Kelland et al., 2020; Vienne et al., 2022; Beerling et al., 2020) and mining tailings (Bea et al., 2012; Nowamooz et al., 2018). Focusing on ERW on cropland, Kelland et al. (2020) developed a reactive transport modeling framework to predict carbon drawdown in soil amended with basaltic dust.

Previous laboratory (Khalidy et al., 2023) and field-scale (Haque et al., 2023) studies have highlighted the downward migration of carbonates in the soils amended with crushed wollastonite. However, no reactive transport modeling has been employed to investigate the long-term fate of products of wollastonite weathering in soil. To meet this objective, we have developed a reactive transport modeling framework through the X1t module of The Geochemist Workbench (GWB) software package. In this chapter, the potential long term carbon drawdown of ERW practice due to wollastonite application along with the model's parameters configuration is presented.

## 2. Methods

## 2.1 Conceptual model of pedogenic carbonate formation and transport due to enhanced weathering in agricultural soils

Due to its high dissolution rate, wollastonite has been highlighted as a promising candidate for passive carbon sequestration in agricultural soils (Haque et al., 2020). However, the chain of processes concluding in atmospheric $CO_2$ (ambient $CO_2$ solvation in rainwater, wollastonite dissolution, and pedogenic carbonate formation) is a function of several environmental factors (Khalidy et al., 2022).

Figure 1 denotes the hydrological processes affecting water percolation and infiltration through the soil medium as well as reactions expected to occur in the soil and subsoil due to the application of wollastonite to the soil. Under the humid climate regime of southwestern Ontario, the precipitation (rainfall and snowfall) is the leading factor affecting the weathering process on the surface of agricultural soil. Furthermore, several hydrological factors determine flow in the vadose zone in this area.

Accordingly, the water content and movement of water through the soil profile determine the rate of wollastonite weathering and carbon intake in the experimental micro plot. The water infiltration and percolation in soils are affected by a variety of hydrological cycle elements (such as precipitation, evapotranspiration, infiltration, runoff etc.). Infiltration, the rate at which water enters the soil, is controlled by several factors (e.g., soil texture, soil water content, rate of airflow, etc.) (Zeitoun et al., 2021). Within the soil medium, the difference of total soil pore water pressure is decisive on the direction of water migration (Al-Kaisi et al., 2017).

The $CO_2$ dissolved in the system may originate from the atmosphere, decomposition of soil organic matter, or root respiration (Bethke, 2007; Ferdush and Paul, 2021; Haque et al., 2020). Higher contents of neo-formed carbonates were detected in finer fractions of agricultural soils amended with wollastonite (Dudhaiya et al., 2019). On the other hand, the application of finer material may ease the downward migration of sequestration products due to effortless immobilization. Furthermore, a portion of silicate particles may move before reacting with dissolved carbonate and bicarbonate ions. The latter provides feedstock for carbon capture in the subsoil once the favorable geochemical conditions (e.g., range of pH and $CO_2$ enriched solution) are met (Bethke, 2007).

The model developed is comprised of long-term weathering of wollastonite in agricultural soil. Our primary objective is to develop the model based on the local characterization of the experimental micro plot located in Woodstock, southwestern Ontario. Hence, the majority of model input is assigned based on properties of soil and local climatic data of the site.

## 2. Software Overview

The reactive transport modeling is built using the X1T (1D reactive transport) Module of Geochemist's Workbench (GWB) software. The software is developed by Aqueous Solutions LLC located at the University of Illinois at Urbana-Champaign (Bethke et al., 2018). The core of the reactive transport model of the software is based on coupling subsurface flow and transport model with chemical reactions (Bethke and Yeakel, 2016). GWB interprets transport through the movement of groundwater as well as dissolved chemicals through advection, hydrodynamic dispersion, and molecular diffusion mechanisms (Bethke and Yeakel, 2016; Yuan et al., 2017). The software has the capability to model a wide variety of chemical reactions in natural and engineered systems (Bethke and Yeakel, 2012).

The simulation comprises of the React and X1T modules of GWB. A brief summary of each module is provided in the subsequent sections. It is worth mentioning that X1T is similar to React in terms of geochemical reactions it can model, except X1T calculates transport of elements of the system as well.

### 2.2.1 React

React simulates the geochemical processes in the presence of aqueous fluid. Equilibrium distribution of aqueous species in a fluid and saturation state of minerals present in the system are examples of calculations performed with React. This module is dedicated to conducting reaction path modeling (forward modeling) track reactions progress in terms of kinetic paths (reaction of progress over time), titration paths (where reactants are gradually added to the system), polythermal paths (tracing reaction over a range of temperatures) and sliding paths (tracing reaction when species activities or gas fugacity varies) (Bethke and Yeakel, 2012).

To start modeling using React, the initial condition of the system must be defined. Then, all minerals and fluids present in the system (and their respective characteristics) should be determined. The modeling starts with calculating the initial equilibrium state of the system. Then, all changes in the system induced by the change in adding or removing reactants (e.g., dissolution/precipitation of minerals), system's thermal modification, change in fluid/gas composition should be taken into account in system modification. The reaction progress can be demonstrated through a parameter called reaction progress variable (ξ), ranging between 0 (initial system) and 1 (end of reaction) (Bethke and Yeakel, 2012). Furthermore, tracing the reaction progress in terms of elapsed time is feasible in the case of kinetic modeling. The inputs of the model in terms of different tabs customized in the software are explained below (Bethke and Yeakel, 2012).

### 2.2.2 X1T (1D Reactive transport)

To build up a reactive transport model in the software, an initial condition of the domain and the composition and flow rate of the fluid should be identified (Bethke and Yeakel, 2016; Yuan et al., 2017). Reactive transport modeling comprises of two sections: transport and reaction simulation. While the reaction element behaves similarly to the React module, the transport accounts for the movement of chemical species through different transport mechanisms such as advection (through groundwater movement), hydrodynamic dispersion, and molecular diffusion. Accordingly, the initial condition (mineralogy of the system and chemical composition of pore fluid) has to be set for performing the modeling.

## 2.3 Model configuration for building reactive transport modeling

To build up a reactive transport model through the X1T module, several parameters should be imported into the model in different panes (Initial, Interval, Fluids, Flow, Reactants, Domain, and Medium).

### 2.3.1 Initial condition

In this section, all components of the system, including solvent (aqueous fluid), minerals, and gases, are identified and treated as an equilibrium model (as the state of system at the beginning of the simulation). The temperature of the system, duration of the simulation (in the case of kinetic modeling), and fluid properties (density and total dissolved solids) are the other parameters that might need to be imported into the system.

## 2.3.2 Interval, Fluids and Flow

As the simulation proceeds, an unreacted fluid with a certain composition passes over the domain (1-D or 2-D) in either linear, radial, or spherical coordinates (Bethke and Yeakel, 2016). In the interval tab, the number and duration of irrigation intervals considered in the system are defined. The chemical composition of inlet solution(s) (unreacted fluid(s)) is set in the “Fluid” tab. In the “Flow” pane, the flow of inlet solutions is set in terms of specific discharge or (indirectly) hydraulic head or potential drop across the domain.

## 2.3.3 Domain and Medium

In the “Domain” tab, the dimensions of the modeling domain are defined. The domain is split into equal elements called “nodal block” and the medium properties of porous media (e.g., porosity, diffusion coefficient, inert volume etc.) are defined in the “Medium” pane for each block. (Bethke and Yeakel, 2016; Yuan et al., 2017).

## 2.3.4 Reactants

As mentioned earlier, the GWB is capable of performing several forms of reaction-path modeling. However, since the kinetic rate law controls the weathering of minerals in the soil-water system, this type of modeling is a matter of interest for our case and is be discussed here.

As soon as a mineral is introduced to a kinetic modeling framework in GWB, the corresponding rate law of the mineral should be set. There are several forms of rate laws that can be defined for GWB, including built-in and custom laws (Bethke et al., 2018). The most common method for calculating the rate law of mineral dissolution and precipitation in geochemical modeling (including GWB) is using transition state theory (TST) (Hellevang et al., 2013; Tole and Lasaga, 1984) as formulated below:

$$r_n = \pm A_n K_n \left| 1 - \left( \frac{Q}{K} \right)^{\theta} \right|^{\eta} \quad (1)$$

Where n, $r_n$, $A_n$, $K_n$ are mineral index, reaction rate (mol/s, positive and negative for dissolution and precipitation, respectively), mineral’s surface area ($cm^2$), and rate constant ($mol/cm^2$ sec), respectively. Q and K are the activity product and equilibrium constant for dissolution reaction, respectively. θ and η are experimentally derived parameters, usually assumed to be unity, called the linear transition state theory rate law (L-TST). In this condition, the reaction might occur faster compared to a natural fluid-water system (Yuan et al., 2017).

According to this equation, when the mineral is undersaturated, it starts to dissolve, and when it is supersaturated it begins to precipitate. Both reactions are a function of rate constant and surface area. Unless a different rate law method is used, all the mentioned parameters should be imported to the model. One deficit with this form of reaction rate is neglecting the impact of the temperature on reaction progress. Therefore, a temperature-dependent rate constant and pH-dependent equation, formulated by Palandri and Kharaka (2004) was used for this simulation. Accordingly, the reaction rate of each mineral is calculated through summation of the rates of the individual mechanisms as follows:

$$k = k_{25}^{nu} \exp\left[ \frac{-E_a^{nu}}{R} \left( \frac{1}{T} - \frac{1}{298.15} \right) \right] + k_{25}^{H} \exp\left[ \frac{-E_a^{H}}{R} \left( \frac{1}{T} - \frac{1}{298.15} \right) \right] a_H^{n_H} + k_{25}^{OH} \exp\left[ \frac{-E_a^{OH}}{R} \left( \frac{1}{T} - \frac{1}{298.15} \right) \right] a_{OH}^{n_{OH}} \quad (2)$$

In this equation, nu, H, and OH labels indicate neutral, acid, and base mechanisms, respectively. E, R, T, a, and n are activation energy, gas constant, absolute temperature (°K), activity of the species, and the power constant. $K_{25}$ is a rate constant at 25° C, respectively.

Palandri and Kharaka (2004) compiled kinetic data for a wide variety of minerals based on experimental data in the literature that have been employed in previous studies.

## 2.4 Initial parameterization, sensitivity analyses, and best fit parameters

To model carbon sequestration in the soil profile due to wollastonite treatment, we built up a model based on the characteristics of the soil column experiment (Khalidy et al., 2023). The 60-cm long soil column setup was divided into 16 cells of 3.75 cm height. The mineral phases (with more than 1%) detected by X-ray diffraction (XRD) quantification were included in the model as the phases. This includes quartz, k-feldspar, albite and microcline, and muscovite. As discussed in Khalidy et al., 2023, the wollastonite ore used in the experiment contains both wollastonite and diopside. Hence, these minerals were added up as additional mineral phases into four top layers (node 1–4) of the modeling framework. It should be mentioned that based on stoichiometry calculation, 53.03 wt% (47.72 gr) and 22.10 wt% (19.87 gr) of applied wollastonite skarn was pure wollastonite and diopside, respectively (other (27.10 wt%) being the sum of other minor phases such as FeO, $Na_2O$, $K_2O$, and $SiO_2$ identified using XRD and XRF). Therefore, the net amount of these minerals was considered in the modeling. Using a physisorption analyzer (Quantachrome Autosorb iQ), the multipoint Brunauer-Emmett-Teller (BET) surface area of wollastonite ore was determined (8560 $cm^2/gr$). All native soil mineral phases were modeled according to the rate laws compilation reported by Palandri and Kharaka (2004). The parameterization for these mineral phases is tabulated in Table 1. The surface area of the mentioned mineral phases was acquired from the literature (Bethke, 2007).

Table 1. Mineralogy of soil minerals phases and their rate law parameters considered in the modeling

| Mineral | Volume (%) | Acid Mechanism | | | Neutral Mechanism | | Base Mechanism | | |
|---|---|---|---|---|---|---|---|---|---|
| | | Log k[a] | E[b] | n | Log k | E | Log k | E | n |
| Albite ($NaAlSi_3O_8$) | 19 | -10.60 | 65 | 0.457 | -12.56 | 69.8 | -15.6 | 71 | -0.57 |
| K-feldspar ($KAlSi_3O_8$) | 14 | -10.00 | 51.7 | 0.5 | -12.41 | 38 | -21.20 | 94.1 | -0.82 |
| Muscovite ($KAl_2(AlSi_3O_{10}(FOH)_2)$) | 4 | -11.85 | 11 | 0.37 | -13.55 | 22 | -14.55 | 22 | -0.22 |
| Quartz ($SiO_2$) | 63 | -9.98 | 37.9 | 0.31 | -13.99 | 87.7 | -14.96 | 87.7 | -0.41 |

[a] Rate constant k at 25°C, pH = 0, mole $m^{-2}$ $s^{-1}$

[b] Arrhenius activation energy, kJ $mole^{-1}$

The “V8.R6+” thermodynamic database was used to build the reactive transport model. An equilibrium between atmospheric $CO_2$ and dissolved inorganic carbon species was considered similar to previous studies (Kelland et al., 2020; Vienne et al., 2022). As $CO_2$ concentration in the soil is higher than the atmospheric level, the soil carbon concentration was used and converted to partial pressure over the vertical profile of soil (Nan et al., 2016). The composition of the initial fluid was set according to the efflux of control columns of the experiment. The flow and interval of irrigation were estimated according to the pattern conducted in the experiment (e.g., irrigation of the column every 3–4 days). The balance between mineral, fluid, and gaseous phases in each nodal block was set based on experimental data (e.g., volumetric moisture content, bulk density, moisture content, etc.) obtained during the soil column experiment. The volume of effluent in the experimental study was used as the inlet fluid of the system.

For wollastonite and diopside kinetic rate law, we initially intended to use data reported by Palandri and Kharaka (2004). Another experimental-based rate law was also investigated to see if the model is sensitive to this configuration. For calcite, we investigated two scenarios for the dissolution/ precipitation of calcite: through the equilibrium phase and the rate law mentioned in Table 2 (Chou et al., 1989).

Table 2. Kinetic rate law parameters of silicate minerals (wollastonite and diopside) and calcium carbonate

| Mineral | Acid Mechanism | | | Neutral Mechanism | | Reference |
|---|---|---|---|---|---|---|
| | Log k | E | n | Log k | E | |
| Diopside ($MgCaSi_2O_6$) | -6.36 | 96.1 | 0.71 | -11.11 | 40.60 | Palandri and Kharaka (2004) |
| Wollastonite ($CaSiO_3$) (I) | -5.37 | 54.7 | 0.40 | -8.88 | 54.7 | |
| Other rate laws: | | | | | | |
| Wollastonite ($CaSiO_3$) (II) | $r_{n+} = SA(10^{-11.41}{a_{H+}}^{0.18})$ | | | | | Schott et al., (2012) |
| Calcite ($CaCO_3$) | $r_{n+} = SA(10^{-0.051}a_{H+} + 10^{-6.19}a_w + 10^{-3.301}a_{H2CO3(aq)})(1 - \raisebox1ex\$Q\$/\raisebox-1ex\$K\$)$ | | | | | Chou et al., (1989) |

Cation exchange capacity (CEC) is another process that has been included in the previous reactive transport models focused on ERW in soil system (Kelland et al., 2020; Vienne et al., 2022). It is possible to define the ion exchange on mineral surfaces in the GWB through the TEdit module and define the amount of sorbing surface. For estimating CEC, we used the regression models developed based on soil characteristics (e.g., particle size, soil organic matter, and pH) (Khaledian et al., 2017).

Aside from the mentioned parameters, other parameters needed to be identified in the reactive transport module of the GWB include diffusion coefficient and longitudinal dispersivity. Though measured in the literature (Vanderborght and Vereecken, 2007; Nan et al., 2016; Fan and Jones, 2014), the reported range for these parameters is broad, and we needed to find the best fit value according to the experimental results.

Before determining the fittest parameters, a series of sensitivity analyses were conducted to determine which parameters are influential on the parameters of interest (e.g., carbonate content of soil, Mg and Ca concentration in the effluent, pH of soil, and effluent).

Once the most influential variables were determined in the sensitivity analyses, the reactive transport model was run for the same duration as that of our experimental study to figure out the best fit parameters. Different scenarios were investigated, and their results were compared to experimental data.

## 2.5 Long-term simulations

Once the best-fitted parameters were established, the model was run for different scenarios over long term (e.g., 5 years). This includes assessing the impact of irrigation flow and the evolution of pedogenic carbonates over the vertical profile of soil.

## 3. Results and discussion

# 3.1 Sensitivity analyses and best fitted parameters

Table 3 presents the parameters included in the sensitivity analyses. The system's moisture content (fluid volume) can not be directly calculated in the GWB. One of the infiltration models found appropriate for the case study was recently developed by Wang and Chu (2020). This model is a revised version of the Horton infiltration model that has been widely used in literature and is capable of simulating the infiltration process during an event (as is the case of our simulation) and continuous conditions. This model imports a few parameters based on climate records (rainfall and potential evaporation) and soil parameters (soil's texture, water capacity properties). The output of this model is infiltration and water content in various layers that can be incorporated into the GWB reactive transport modeling framework as the initial condition of modeling. Also, this model was run for the experimental condition of our experiment (160 days), the change in moisture content was so small that the variation wasn't included in the reactive transport modeling. However, two scenarios of lower (-5%) and higher (5%) moisture content were assessed in the sensitivity analyses.

**Table 3. Parameters (and the range of interest) investigated in the sensitivity analyses**

| Parameter | Range of variable | References |
|---|---|---|
| Moisture content | ± 5% of experimental results | - |
| Irrigation regime | 5%, 10%, 15%, constant flow | - |
| CEC | 10–45 (meq/100 gr) | Khaledian et al., (2017) |
| Diffusion coefficient | 0.005 to 0.01 ($cm^2/s$) | Nan et al., (2016), Fan and Jones (2014) |
| Longitudinal dispersivity | 3–12 (cm) | Vanderborght and Vereecken (2007) |

We planned to replicate the intermittent irrigation regime (same as experimental condition) with repeating injections of water every 3–4 days. In this case, the flow rate had to be to "zero" for each dry spell. However, the software is not able to proceed with these settings, and the simulation crashes out. To solve this problem, a few scenarios were considered. The first scenario assumes the flow rate is constant over the course of the reaction ("constant" in Fig. 2). In this case, called "constant flow", the total volume of injected water was assumed to be irrigated uniformly during the experiment (the flow rate of dry and wet spells was considered to be the same). In other scenarios, it was assumed a small ratio (e.g., 5,10,15%) of effluent volume was injected into the domain over the dry spell, while the remnant (e.g., 95,90,85%) was injected during the wet spell. The specific discharge evolution over the simulation period (same as the experiment) for different scenarios is denoted in Fig. 2.

For other parameters (CEC, diffusion coefficient, longitudinal dispersivity), a range of values reported in literature was investigated. Also, for CEC, we ran a scenario without any ion exchange as well.

**Table 4. Best-fitted parameters determined on the basis of comparison with experimental results**

| Parameter | Values/ rate expression |
|---|---|
| Flow rate (wet spell, dry spell) (cm/day) | 1.875, 0.032 |
| CEC (meq/100 gr) | 15 |
| Longitudinal dispersivity (cm) | 10 |
| Fitted calibration factor (Wollastonite) | 0.07 |
| Wollastonite dissolution rate law | $r_{n+} = SA(10^{-11.41}.{a_{H+}}^{0.18})$ |
| Calcite dissolution rate law | Modeled as an equilibrium phase |

The results of sensitivity analysis show the model results vary with changing all of the parameters except diffusion coefficients and moisture content. The degree of change is different for each parameter and varies between 5–10% (for irrigation regime) to 1000% (for CEC). We also noticed that the variability of pH (both of leachate and soil) is narrow for most of parameters. Hence, we didn't include pH in the best-fit parameters simulations.

To determine the best fit parameters for the simulation, another set of simulations was run, and the parameters represented in Table 4 were concluded as the best-fit parameters for the modeling. The fitted calibration factor indicates the ratio of reactive surface area to measured surface area and is in the range of 0.001 to 0.1 for reactive silicate minerals (Bea et al., 2012). After investigating a wide range of values (0.0001 to 0.1), we determined this factor for wollastonite to be 0.07. Regarding wollastonite/diopside dissolution kinetic rate, both investigated rate laws (Palandri and Kharaka, 2004; Schott et

al., 2012) showed reasonable results, particularly for pH > 7, with higher amounts of dissolution for wollastonite for pH < 6 with Palandri and Kharaka (2004) data. However, Schott et al. (2012) data were used as it was a slightly better match with experimental observations data.

## 3.2 Short term simulation

Once the best fit parameters were determined for the modeling framework, we ran the model for 160 days (the duration of the experimental study). The difference in Mg and Ca leachate between control and wollastonite amendment (both experimental and modeled) is demonstrated in Fig. 3.

It can be implied that the model initially underestimates the Ca concentration in the leachate, while the trend shifts to overestimation as the experiment proceeds. One explanation for this discrepancy is that the model neglects the fact that the highly reactive portion of the mineral tends to dissolve at first, while after some time, the dissolution rate of the mineral tends to decrease. This trend is evident in the amount of Ca released over time during the experiment. Another remarkable point is that the change in flow regime (shifting from the dry to the wet spell) affects the simulated Ca concentration in the effluent.

Focusing on Mg content, the model initially overestimates the dissolution of diopside, while the trend tends to be underestimated as the modeling proceeds. The observed data shows Mg concentration is pretty consistent over the experiment (considering the scale, most of the observations fall in less than 2 mg/l range). In the study conducted by Vicca et al. (2022), their reactive transport model underestimated the concentration of both Ca and Mg in the soil pore water, with a lower magnitude in the latter. The model slightly underestimated carbonate content accumulation in soil treated with wollastonite. The same pattern was observed in the model developed through PHREEQC software (Vicca et al., 2022).

## 3.3 long term simulation

### 3.3.1 Extending the experimental condition to long term

With running forward the reactive transport model, the long-term sequestration pattern of $CO_2$ is simulated and demonstrated in Fig. 4. Accordingly, the calcite precipitation rate is dominant at the beginning of the reaction (first year), and it goes on a quite linear decline after that. Once parts of reactive silicate minerals are dissolved in the system, the pH of system increases and go beyond 7.5 (the initial pH of the soil was between 6.3 and 6.5). The dissolution of wollastonite and diopside is limited in the pH > 7 range, slowing down the precipitation of calcite and eventually dissolving (and recrystallizing) some of the calcite in the system. The effluent of carbonates in the leachate system is small initially, but it continues to grow at a constant rate throughout the simulation. The results are in agreement with Kelland et al. (2020)'s previous study where that formation of carbonate was dominant at the beginning of the simulation due to amendment with a basaltic dust (enriched in diopside), while the bicarbonate pool tended to grow over time. They estimated a comparable carbon sequestration rate (5 t/ha) after five years in the soil column, with a rock powder dosage of 100 t/ha.

### 3.3.2 Investigating impact of inflow (precipitation)

Since the previous section described a specific flow rate (rainfall pattern), two more scenarios (with ± 50% flow rate) were investigated to see the impact of the inflow into system. The results are shown in Fig. 5. Accordingly, the lower the inflow, the higher pedogenic carbonate formation in the system.

In the lower flow rate scenario, it is implied that not only is more calcite initially formed in the system, but also the dissolution rate of calcite in the systems is lower over time. To have closer look at the high inflow scenario, the evolution of sequestered carbon in the forms of carbonate precipitation and effluent flux of bicarbonate is demonstrated in Fig. 6. This plot shows that even at higher flow rate carbonate precipitation is dominant at the initial stage of simulation, while as the modeling proceeds dissolved carbonate/bicarbonate grows and exceeds the solid carbonate in the system. However, it is evident that even in high flow rate scenario (equivalent to more than 2000 mm/year), the formation of pedogenic carbonate is significant and should be considered as a sink for the ERW process.

Figure 7 depicts the dissolution trend of minerals (wollastonite and diopside) as the same in all three scenarios (all corresponding lines of given minerals overlap with each other in all scenarios). It can be deduced that flow rate doesn't influence the dissolution of mineral, however, it controls precipitation and re-dissolution of calcite and effluent flux of weathering product (e.g., bicarbonate and Ca and Mg).

According to Fig. 5, the newly formed carbonate is comparatively persistent in the low-inflow scenario. The evolution of pedogenic carbonate formed due to wollastonite amendment over the vertical profile of soil and the course of simulation is demonstrated in Fig. 8. It can be concluded that at the initial stage of simulation (0–2 years), carbonate accumulated in 0–15 cm layer, with limited formation in deeper layers. As the modeling proceeds, the carbonates migrate and redistribute over the profile of soil. Eventually, at the end of modeling (5th year), a more uniform distribution of carbonate is forming over the vertical soil profile. It should be noted that as the simulation proceeds, the total amount of carbonates decreases in the system, and the carbonate leaves the system in the dissolved form (as discussed earlier and shown in Fig. 6).

## 4. Conclusion

Here, we developed a reactive transport model configured on the basis of experimental observations to estimate long-term fate of weathering products over a soil profile during ERW practice. The most influential and best-fitted parameters (e.g., fitted calibration curve, the kinetic dissolution rate of reactive minerals, irrigation regime, etc.) were determined through two series of sensitivity and best-fitted parameters analyses, respectively. The short-term results showed that wollastonite and diopside dissolution were higher at the beginning of the simulation. As the pH elevates, the dissolution of reactive minerals decelerates, and less cations ($Ca^{2+}$ and $Mg^{2+}$) leave the system as efflux. The long-term results indicate continuing weathering in soil for a long period

(e.g., a few years) so that all reactive minerals (wollastonite and diopside) are dissolved in the soil-water system. The carbonate formation and migration were found to be a function of the irrigation regime. Where higher inflow rates ease movement of dissolved cations and carbonates through efflux, while lower inflow leads to higher carbonate formation (in form of solid) and less mobilization of weathering products in the system. Investigating the vertical distribution of newly formed carbonate over the soil profile denoted that carbonate accumulates in the top layer (e.g., 0–15 cm) at the initial stage of simulation (first and second year). From a longer perspective, carbonate migrates to deeper layers through the dissolution/recrystallization process, while a small portion of dissolved carbonates leaves the column through the effluent.

## References


1. Al-Kaisi, M.M., Lal, R., Olson, K.R., Lowery, B., 2017. Fundamentals and Functions of Soil Environment. Soil Heal. Intensif. Agroecosystems 1–23. https://doi.org/10.1016/B978-0-12-805317-1.00001-4
2. Beerling, D.J., Kantzas, E.P., Lomas, M.R., Wade, P., Eufrasio, R.M., Renforth, P., Sarkar, B., Andrews, M.G., James, R.H., Pearce, C.R. and Mercure, J.F., 2020. Potential for large-scale CO2 removal via enhanced rock weathering with croplands. Nature, 583(7815), pp.242-248. https://doi.org/10.1038/s41586-020-2448-9.
3. Bea, S.A., Wilson, S.A., Mayer, K.U., Dipple, G.M., Power, I.M., Gamazo, P., 2012. Reactive transport modeling of natural carbon sequestration in ultramafic mine tailings. Vadose Zone. J. 11. https://doi.org/10.2136/vzj2011.0053 vzj2011.0053.
4. Bethke, C.M., Farrell, B., Yeakel, S., 2018. The Geochemist's Workbench, Version 12.0: GWB Essentials Guide. Aqueous Solutions. Illinois, US LLC Champaign.
5. Bethke, C.M., Yeakel, S., 2016. GWB reactive transport modeling guide.
6. Bethke, C.M., Yeakel, S., 2012. The Geochemist's Workbench (Version 9.0): Reaction modeling guide. Aqueous Solut. LLC, Champaign, Ill.
7. Campbell, J.S., Foteinis, S., Furey, V., Hawrot, O., Pike, D., Aeschlimann, S., Maesano, C.N., Reginato, P.L., Goodwin, D.R., Looger, L.L., Boyden, E.S., Renforth, P., 2022. Geochemical negative emissions technologies: part I.Review. Front. Clim. 4, 133. https://doi.org/ 10.3389/fclim.2022.879133.
8. Chou, L., R.M. Garrels, and R. Wollast. 1989. Comparative study of the kinetics and mechanisms of dissolution of carbonate minerals. Chem. Geol. 78:269–282. doi:10.1016/0009-2541(89)90063-6.
9. Fan, J., Jones, S.B., 2014. Soil surface wetting effects on gradient-based estimates of soil carbon dioxide efflux. Vadose Zone J. 13 (2), 53-63. https://doi.org/10.2136/vzj2013.07.0124.
10. Goll, D.S., Ciais, P., Amann, T., Buermann, W., Chang, J., Eker, S., Hartmann, J., Janssens, I., Li, W., Obersteiner, M., Penuelas, J., Tanaka, K., Vicca, Sara., 2021. Potential $CO_2$ removal from enhanced weathering by ecosystem responses to powdered rock. Nat. Geosci. 14, 545–549.
11. Haque, F., Khalidy, R., Chiang, Y.W., Santos, R.M., 2023. Constraining the Capacity of Global Croplands to CO2 Drawdown via Mineral Weathering. ACS Earth Space Chem., in press. 10.1021/acsearthspacechem.2c00374.
12. Haque, F., Santos, R.M., Chiang, Y.W., 2020. $CO_2$ Sequestration by wollastonite-amended agricultural soils-An Ontario field study. Int. J. Greenh. Gas Control 97, 103017. https://doi.org/10.1016/j.ijggc.2020.103017.
13. Huang, M., Zhai, P., 2021. Achieving Paris Agreement temperature goals requires carbon neutrality by middle century with far-reaching transitions in the whole society. Adv. Clim. Change Res. 12, 281–286. https://doi.org/10.1016/j.accre.2021.03.004.
14. Jariwala, H. Haque, F., Vanderburgt, S., Santos, R.M., Chiang, Y.W., 2022. Mineral-Soil-Plant-Nutrient Synergisms of Enhanced Weathering for Agriculture: Short-Term Investigations Using Fast-Weathering Wollastonite Skarn. Front. Plant Sci. 13, 929457. https://doi.org/10.3389/fpls.2022.929457.
15. Jorat, M.E., Kraavi, K.E., Manning, D.A.C., 2022. Removal of atmospheric CO2 by engineered soils in infrastructure projects. J. Environ. Manage. 314, 115016. https://doi.org/10.1016/j.jenvman.2022.115016.
16. Kelland, M.E., Wade, P.W., Lewis, A.L., Taylor, L.L., Sarkar, B., Andrews, M.G., Lomas, M.R., Cotton, T.E.A., Kemp, S.J., James, R.H., 2020. Increased yield and $CO_2$ sequestration potential with the C4 cereal Sorghum bicolor cultivated in basaltic rock dust-amended agricultural soil. Glob. Chang. Biol. 26, 3658–3676. https://doi.org/10.1111/gcb.15089.
17. Khaledian, Y., Brevik, E.C., Pereira, P., Cerda`, A., Fattah, M.A., Tazikeh, H., 2017. Modeling soil cation exchange capacity in multiple countries. Catena. 158, 194–200. https://doi.org/10.1016/j.catena.2017.07.002
18. Khalidy, R., Arnaud, E., Santos, R.M., 2022. Natural and Human-Induced Factors on the Accumulation and Migration of Pedogenic Carbonate in Soil: A Review. Land 11, 1448. https://doi.org/10.3390/land11091448.
19. Khalidy, R., Chiang, Y.W., Santos, R.M., 2023. Fate and migration of enhanced rock weathering products through soil horizons; implications of irrigation and percolation regimes. Catena 233, 107524. https://doi.org/10.1016/j.catena.2023.107524
20. Khalidy, R., Haque, F., Chiang, Y.W., Santos, R.M., 2021. Monitoring pedogenic inorganic carbon accumulation due to weathering of amended silicate minerals in agricultural soils. JoVE 2021. https://doi.org/10.3791/61996.
21. Khalidy, R., Santos, R.M., 2021a. The fate of atmospheric carbon sequestrated through weathering in mine tailings. Miner. Eng. 163, 106767. https://doi.org/10.1016/j.mineng.2020.106767
22. Khalidy, R., Santos, R.M., 2021b. Assessment of geochemical modeling applications and research hot spots—a year in review. Environ. Geochem. Health 43, 3351–3374. https://doi.org/10.1007/s10653-021-00862-w

23. La Plante, E.C., Mehdipour, I., Shortt, I., Yang, K., Simonetti, D., Bauchy, M., Sant, G.N., 2021. Controls on CO2 mineralization using natural and industrial alkaline solids under ambient conditions. ACS Sustain. Chem. Eng. 9, 10727–10739. https://doi.org/10.1021/acssuschemeng.1c00838.
24. Nan, W., Yue, S., Li, S., Huang, H., Shen, Y., 2016. The factors related to carbon dioxide effluxes and production in the soil profiles of rain-fed maize fields. Agric. Ecosyst. Environ. 216, 177–187. https://doi.org/10.1016/j.agee.2015.09.032.
25. Nowamooz, A., Dupuis, J.C., Beaudoin, G., Molson, J., Lemieux, J.M., Horswill, M., Fortier, R., Larachi, F., Maldague, X., Constantin, M., Duchesne, J., Therrien, R., 2018. Atmospheric carbon mineralization in an industrial-scale chrysotile mining waste pile. Environ. Sci. Technol. 52, 8050–8057. https://doi.org/10.1021/acs. est.8b01128.
26. Palandri, J.L., Kharaka, Y.K., 2004. A compilation of rate parameters of water-mineral interaction kinetics for application to geochemical modeling. Geological Survey Menlo Park CA.
27. Rausis, K., Stubbs, A.R., Power, I.M., Paulo, C., 2022. Rates of atmospheric CO2 capture using magnesium oxide powder. Int. J. Greenh. Gas Control 119, 103701. https://doi.org/10.1016/j.ijggc.2022.103701.
28. Schott, J., Pokrovsky, O.S., Spalla, O., Devreux, F., Gloter, A., Mielczarski, J.A., 2012. Formation, growth and transformation of leached layers during silicate minerals dissolution: the example of wollastonite. Geochim. Cosmochim. Acta 98, 259–281. https://doi.org/10.1016/j.gca.2012.09.030.
29. Vanderborght, J., Vereecken, H., 2007. Review of dispersivities for transport modeling in soils. Vadose Zone. J. 6(1), 29-52.
30. Vienne, A., Poblador, S., Portillo-Estrada, M., Hartmann, J., Ijiehon, S., Wade, P., Vicca, S., 2022. Enhanced Weathering Using Basalt Rock Powder: Carbon Sequestration, Co-benefits and Risks in a Mesocosm Study With Solanum tuberosum. Front. Clim. 4, 869456. https://doi.org/10.3389/fclim.2022.869456.
31. Wang, N., Chu, X., 2020. Revised Horton model for event and continuous simulations of infiltration. J. Hydrol. 589. https://doi.org/10.1016/j.jhydrol.2020.125215
32. Washbourne, C.-L., Renforth, P., Manning, D.A.C., 2012. Investigating carbonate formation in urban soils as a method for capture and storage of atmospheric carbon. Sci. Total. Environ. 431, 166–175. https://doi.org/10.1016/j.scitotenv.2012.05.037.
33. Wilson, S.A., Harrison, A.L., Dipple, G.M., Power, I.M., Barker, S.L.L., Ulrich Mayer, K., Fallon, S.J., Raudsepp, M., Southam, G., 2014. Offsetting of CO2 emissions by air capture in mine tailings at the Mount Keith Nickel Mine, Western Australia: rates, controls and prospects for carbon neutral mining. Int. J. Greenh. Gas Control 25, 121–140. https://doi.org/10.1016/j.ijggc.2014.04.002.
34. Yuan, G., Cao, Y., Gluyas, J., Jia, Z., 2017. Reactive transport modeling of coupled feldspar dissolution and secondary mineral precipitation and its implication for diagenetic interaction in sandstones. Geochim. Cosmochim. Acta 207, 232–255. https://doi.org/10.1016/j.gca.2017.03.022
35. Zeitoun, R., Vandergeest, M., Vasava, H.B., Machado, P.V.F., Jordan, S., Parkin, G., Wagner-Riddle, C., Biswas, A., 2021. In-situ estimation of soil water retention curve in silt loam and loamy sand soils at different soil depths. Sensors (Switzerland) 21, 1–15. https://doi.org/10.3390/s21020447

## Figures

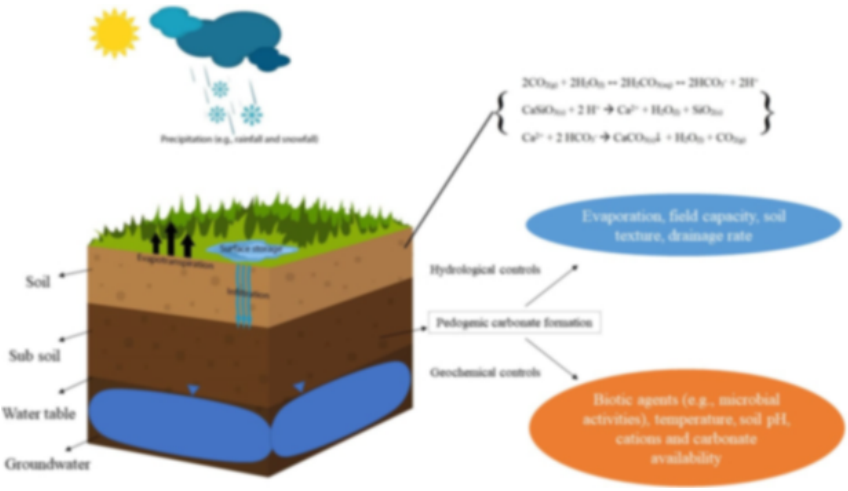


**Figure 1**

**Conceptual model of pedogenic carbonate formation in agricultural soils amended with wollastonite**

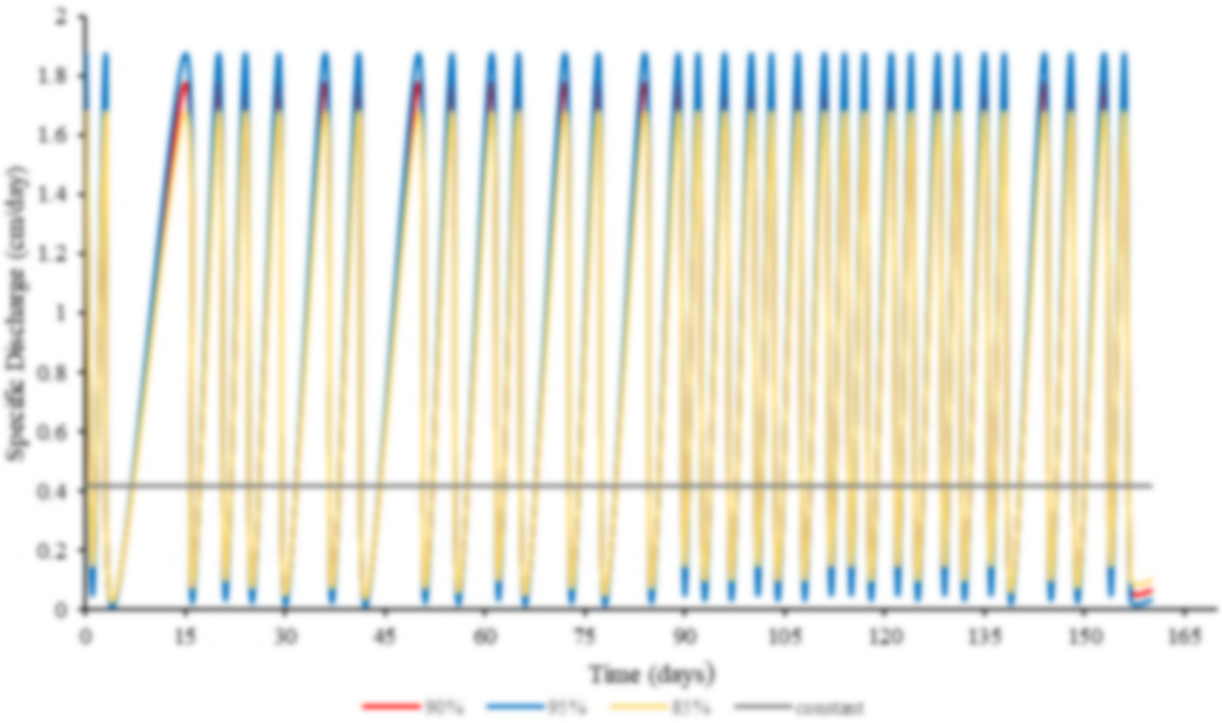


Figure 2

Evolution of specific discharge during different scenarios of the simulation.

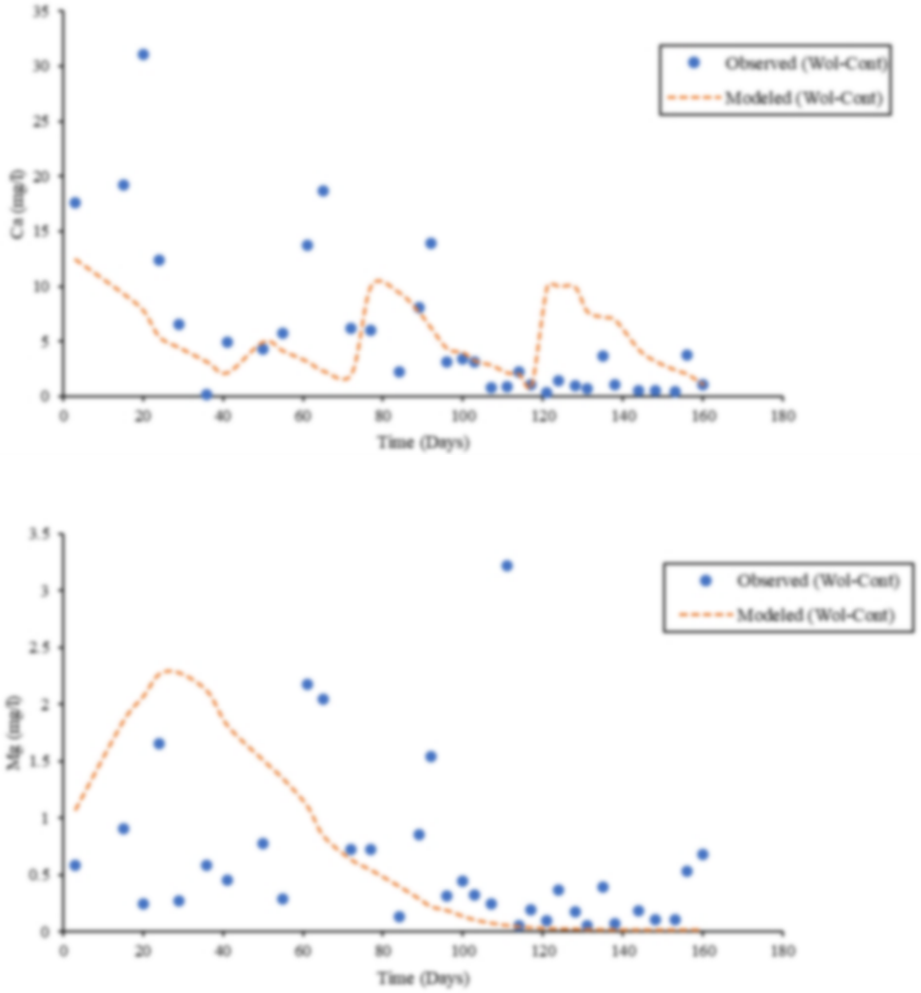


Figure 3

The trend of experimental (observed) and simulated Mg and Ca delta (difference of wollastonite amendment and control) as a function of time (days)

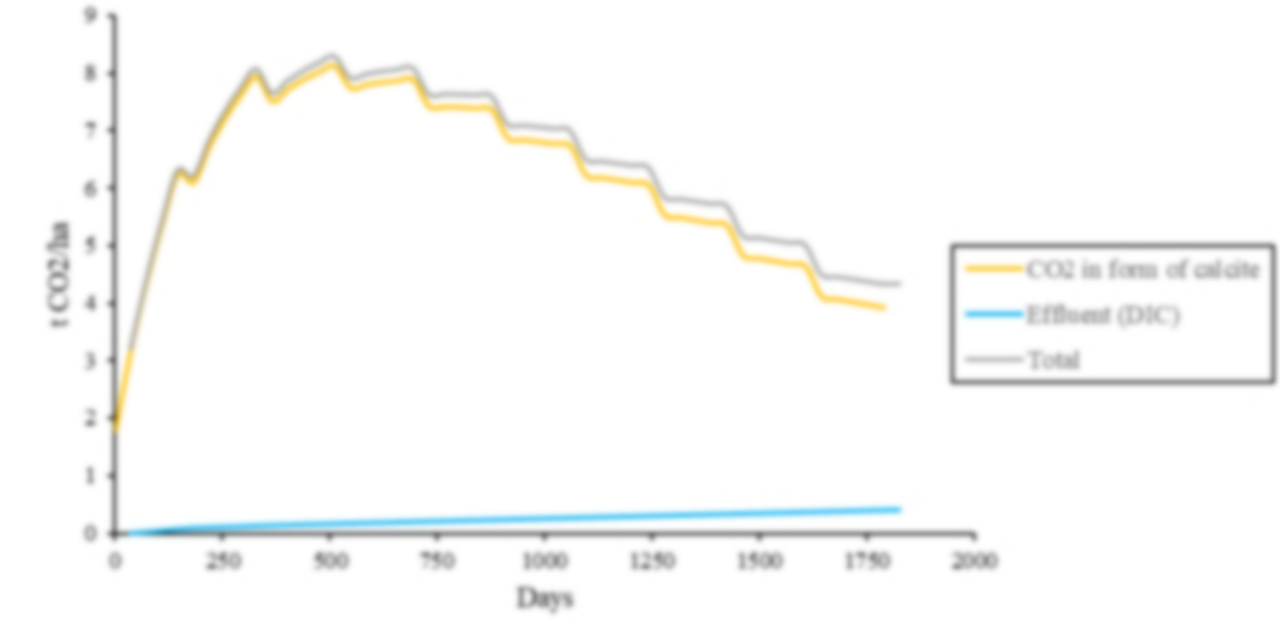


Figure 4

Long-term reactive transport modeling of carbon capture in soil amended wollastonite ore (wollastonite and diopside) weathering

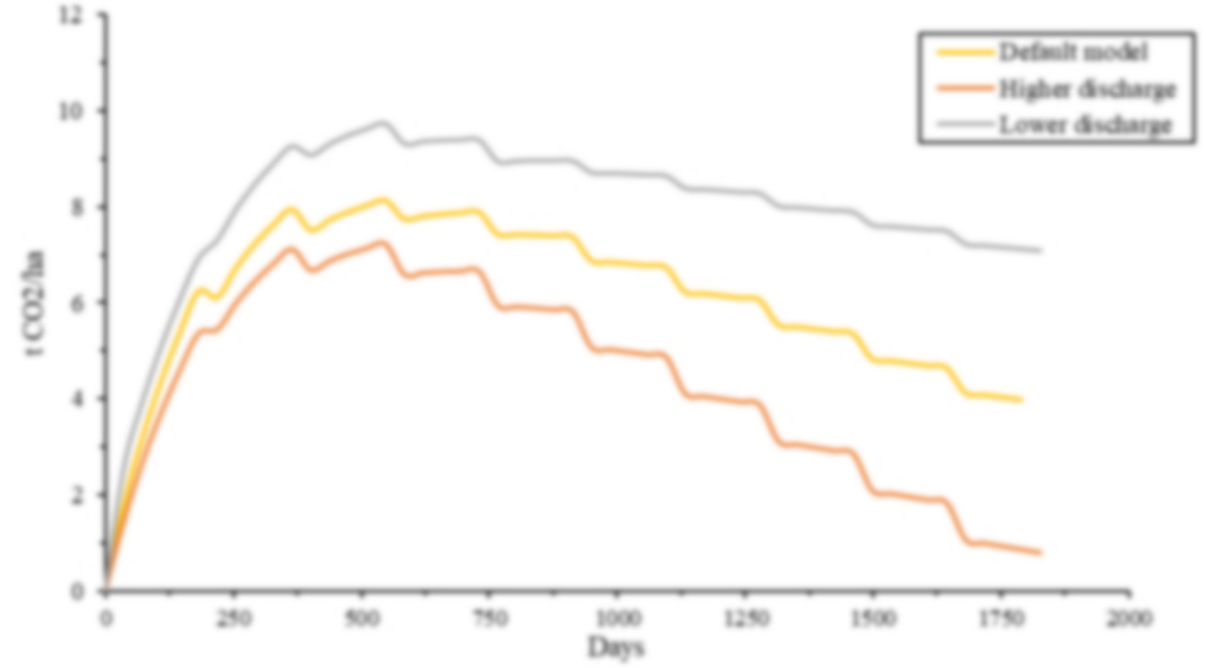


Figure 5

Impact of inflow rate on pedogenic carbonate formation/dissolution in the soil

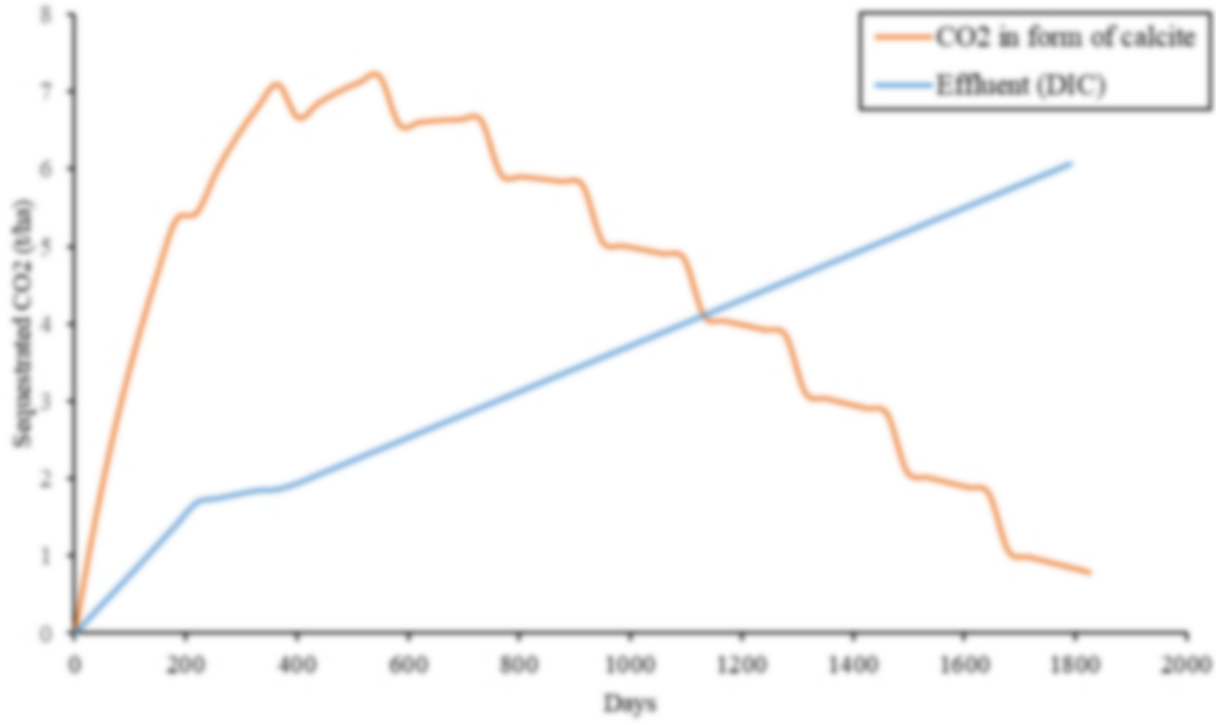


Figure 6

The evolution of sequestrated carbon in forms of carbonate precipitation and effluent flux of bicarbonate (High inflow rate scenario)

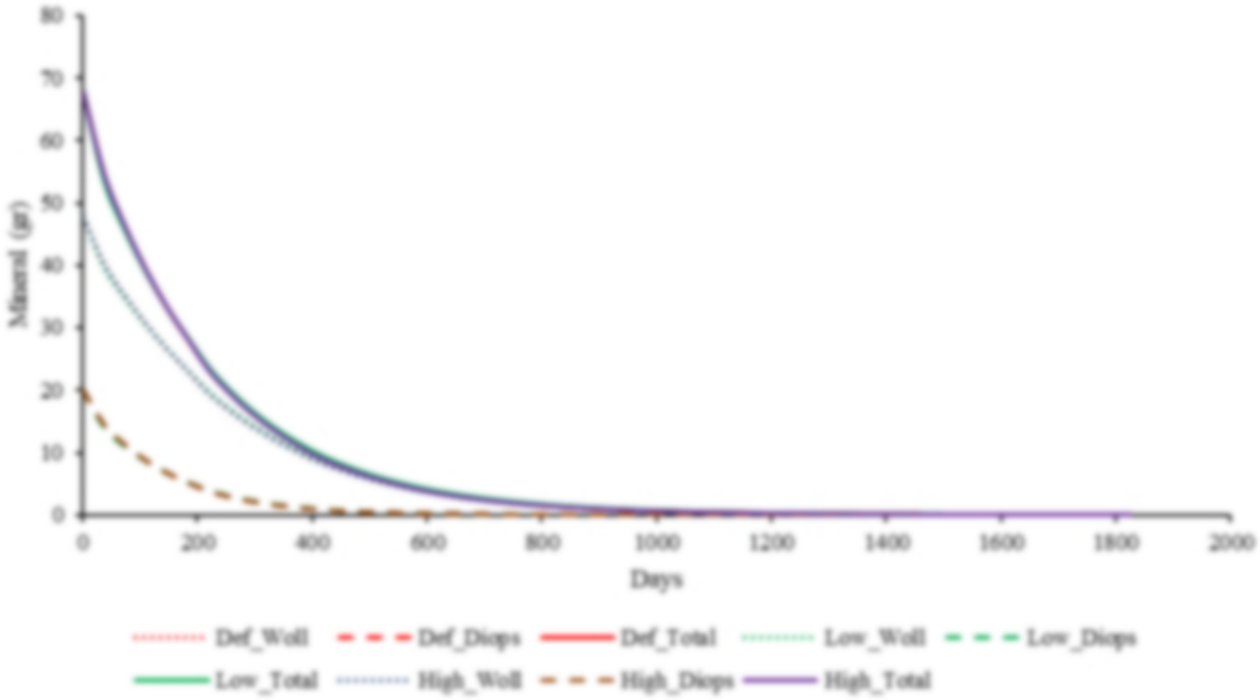


Figure 7

Dissolution of fast-weathering minerals (wollastonite and diopside) over time (High flow rate/default/low flow scenarios)

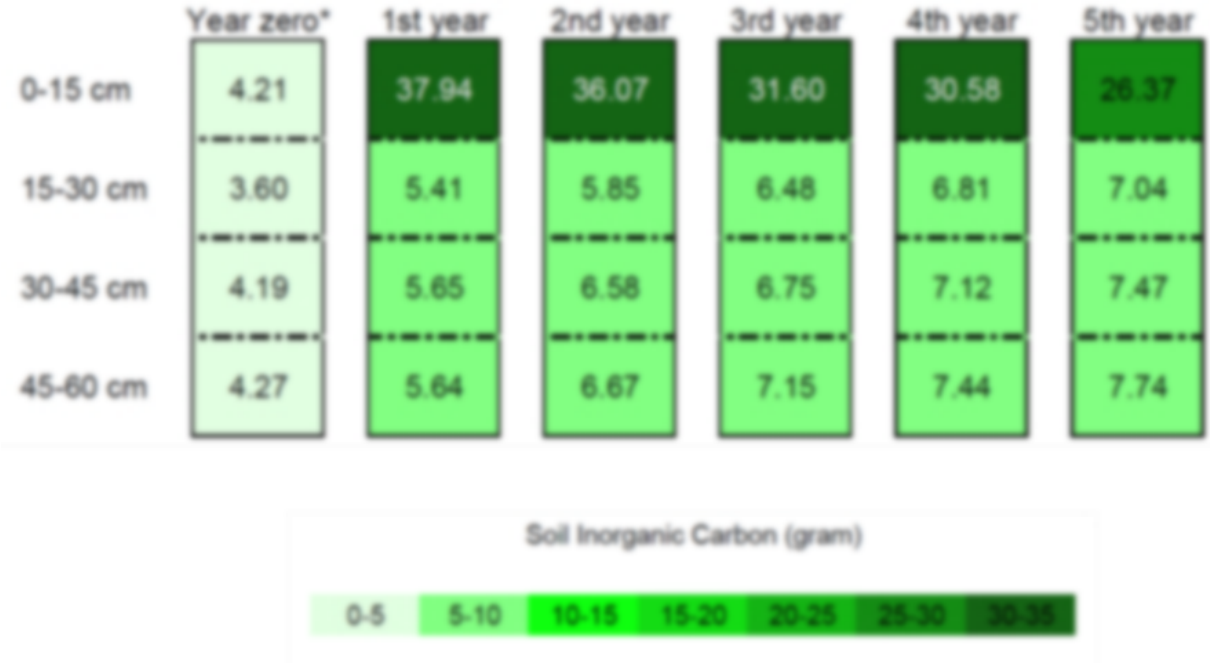


Figure 8

The evolution of pedogenic carbonate formed due to wollastonite amendment over the vertical profile of soil during the simulation (5 years). The number in each box represent carbonate content in the corresponding layer and time.

* Year zero indicates the state, before the simulation beginning